

**A Multigrid Method for Shape from  
Shading <sup>1</sup>**

by

Uri M. Ascher  
Paul M. Carter

Technical Report 91-2  
April, 1991

<sup>1</sup>This research was supported in part under NSERC Canada Grant OGP0004306.



# A Multigrid Method for Shape from Shading<sup>1</sup>

Uri M. Ascher & Paul M. Carter

**Abstract:** The shape-from-shading problem has received much attention in the Computer Vision literature in recent years. The basic problem is to recover the *shape*  $z(x, y)$  of a surface from a given map of its *shading*, i.e. its variation of brightness over a given domain. Mathematically, one has to solve approximately the *image irradiance equation*

$$R(p, q)(x, y) = E(x, y)$$

relating a given image irradiance  $E(x, y)$  to the radiance of the surface at each point  $(x, y)$ , with  $R(p, q)$  a given *reflectance map* which is a usually nonlinear function of  $p = z_x$  and  $q = z_y$ .

A possible presence of noise and lack of adequate boundary conditions adds to the difficulty of this problem. A number of different approaches towards its solution have been proposed in the Vision literature, including various regularization models. However, a reliable, efficient solution method for practical instances has remained elusive so far.

In this paper we analyze the various solution models proposed with the aim of applying an efficient multigrid solver. A combination of an FMG-continuation technique with an appropriate discretization of one such solution model proposed by B. Horn yields an efficient solver. Our results are demonstrated by examples.

## 1 Introduction

The shape-from-shading problem has received much attention in the Computer Vision literature in recent years. A recent book [10] contains a reprinted collection of some of the more important papers on this topic. The basic problem is to recover the *shape*  $z(x, y)$  of a surface from a given map of its *shading*, i.e. its variation of brightness over a given domain. Mathematically, under certain assumptions one has to solve approximately the *image irradiance equation*

$$R(p, q)(x, y) = E(x, y) \tag{1}$$

relating a given image irradiance  $E(x, y)$  to the radiance of the surface at each point  $(x, y)$ , with  $R(p, q)$  a given *reflectance map* which is a function of the surface gradient (orientation),  $p = z_x$  and  $q = z_y$ .

Among problems in Computer Vision which deal with surface reconstruction, this is one of the hardest to solve: In addition to the fact that the solution information is given implicitly, through the often strongly nonlinear hyperbolic equation (1), one has to cope with possible

---

<sup>1</sup>This research was supported in part under NSERC Canada Grant OGP0004306.

inaccuracies in the model  $R(p, q)$ , with a possible presence of noise in the data  $E(x, y)$ , with possible discontinuities in the solution and with a possible lack of adequate boundary conditions.

And yet, the problem is of considerable practical interest, because (i) it arises in connection to collision avoidance of robots with their surroundings and for the purposes of automated inspection tasks, and (ii) it has been demonstrated to be a component of the human vision system and as such merits better understanding [15],[14].

A number of different approaches towards the approximate solution of (1) have been proposed in the Vision literature, including various regularization models. However, a reliable, efficient solution method for practical instances has so far remained elusive.

In this paper we briefly describe the problem (Section 2) and analyse various proposed solution models with the aim of applying an efficient multigrid solver (Section 3). Our analysis leads us to concentrate on one such solution model proposed by B. Horn [9] and on its appropriate discretization. We describe in Section 4 a special version of an FMG algorithm [2] where the regularization parameter is updated within the FMG continuation process. This leads to a very efficient algorithm.

Our results are demonstrated by selected examples, to which the final section of this paper is devoted. We consider the use of one or more images, and the imposition of boundary conditions on the object or on the background. The obtained computed results are promising. We conclude by pointing out some directions for further investigation.

## 2 The Problem

We shall not discuss here the assumptions giving rise to the image irradiance equation (1), but rather assume that it holds (see [8],[10],[12]). The reflectance map  $R(p, q)$  may sometimes be linear, as in a Minnaert surface (which is commonly used to model the moon's surface)

$$R(p, q) = \rho \frac{(1 + p_0 p + q_0 q)}{\sqrt{1 + p_0^2 + q_0^2}} \quad (2)$$

(here  $\rho$ , the surface albedo, and  $(p_0, q_0)$ , the direction towards the light source, are known). But  $R$  is more often nonlinear, as in a Lambertian Surface

$$R(p, q) = \rho \frac{(1 + p_0 p + q_0 q)}{\sqrt{1 + p_0^2 + q_0^2} \sqrt{1 + p^2 + q^2}}. \quad (3)$$

In such a case the hyperbolic equation (1) is highly nonlinear. In more general situations where  $R$  is not known analytically but there is a calibration object available, the reflectance map may be obtained experimentally [18],[19].

Questions of solution existence and uniqueness for (1) arise here nontrivially [10],[4],[5]. For a special case of (3) corresponding to a distant overhead illumination of a Lambertian surface, (1) can be written as the *eikonal equation*

$$z_x^2 + z_y^2 = E^{-2} - 1 \quad (4)$$

For this it has been shown [4] that there is no shape  $z$  corresponding to shadings  $E$  which have too dark a spot on too bright a background. At the other end, it is possible in some circumstances that the same image will have more than one corresponding shape [5],[8].

Practically, the availability of boundary or interface information is an important issue. In some cases,  $z$  is known on a closed curve (not only on the inflow part) forming the boundary of the image (e.g. in the case of an object merging smoothly into a fixed background). In many cases one knows the gradient  $(p, q)$  on such a boundary. In addition, the gradient may be determined directly at a singular point where  $R(p, q)$  has a global maximum (see [8]).

If the scene contains more than one smooth object (e.g. an object sharply distinct from a background, or more than one such objects) then there are a number of smooth images separated by interfaces across which  $z$ ,  $p$  and  $q$  are generally discontinuous. (The location of such interfaces is found by an edge detecting preprocessor and is assumed known here.) Some additional boundary information is provided in the case of an *occluding boundary*, where the surface orientation is known because it is perpendicular to the object's silhouette and lies in a plane parallel to that of the image. This information may however be tricky to incorporate because at least one of  $p$  and  $q$  is infinite on such a boundary (or interface).

### 3 Solution Techniques

The earliest attempt at solving (1) numerically used a method of characteristic strips, in which sets of coupled ODEs for  $x, y, z, p$  and  $q$  are solved to cover the  $(x, y)$ -domain (see [8] and Horn's paper in [10]). However, this method was not very robust in the presence of noise. A variety of regularization methods have subsequently been proposed in which a smoothness penalty term is added to an error functional to be minimized

$$F(p, q) = \int \int_{\Omega} (E - R(p, q))^2 d\Omega \quad (5)$$

where the domain of integration,  $\Omega$ , corresponds to a smooth part (or the union of such parts) of the image under consideration.

Many algorithms proposed in the literature proceed in two stages, the first obtaining the surface orientation  $p(x, y)$  and  $q(x, y)$  and the second recovering the surface  $z(x, y)$  from the given orientation. For the second stage a line integration method or an approximate minimization of the functional

$$\int \int_{\Omega} \{(z_x - p)^2 + (z_y - q)^2\} d\Omega \quad (6)$$

(for given  $p, q$ ) are used. A standard multigrid algorithm may be used to efficiently minimize (6).

If one adds to (5) the penalty term

$$\int \int_{\Omega} \lambda (p_x^2 + p_y^2 + q_x^2 + q_y^2) d\Omega \quad (7)$$

with  $\lambda$  a positive parameter and considers minimizing the resulting functional, then the problem appears to be simpler. The necessary conditions (Euler equations, cf [6]) form a simple

elliptic system of equations. Like (6), this can also be solved by a standard multigrid method. However, it has been realized [10] that the first stage of the solution process must ensure that the orientation map produced should correspond to a physical surface. In other words, it is of little use to provide arrays of  $(p, q)$  values which minimize (5) plus (7) if the obtained  $p$  and  $q$  cannot be integrated to yield an underlying surface  $z(x, y)$ . Horn & Brooks [11] proposed adding a penalty term for non-integrability of the surface slopes, i.e. they considered the minimization of

$$F(p, q) = \iint_{\Omega} \{(E - R(p, q))^2 + \mu(p_y - q_x)^2\} d\Omega \quad (8)$$

Notice that this does not strictly enforce integrability at each point: attempts to do this directly by means of a Lagrange multiplier or by replacing  $(p, q)$  by  $\text{grad}z$  in (5) have not produced convergent schemes.

The equations representing necessary conditions for an extremum of (8) were solved in [11] using a simple Jacobi relaxation and needing many iterations. Our first cut at this problem has in fact involved the application of a multigrid method to this formulation to speed up the process. However, upon analyzing the resulting system of equations, it can be shown to be non-elliptic. This appears to explain the slow convergence reported in [11] (although of course the convergence of a relaxation scheme alone is not expected to be very fast for an elliptic operator either), and also indicates that the multigrid method might not perform very efficiently (but see [16]). We therefore considered the addition of a further term (7) to the functional given in (8), which introduces ellipticity into the model. In order to maintain faithfulness to the underlying physical problem we seek to keep the parameter  $\lambda$  as small as possible. However, it should be noted that this additional term which gives ellipticity to the problem is of the same order as the non-ellipticity integrability penalty term. Hence, it is not possible to reduce  $\lambda$  too much before non-ellipticity effects again become a pronounced difficulty.

The incorporation of boundary value information is an important issue. While the various regularizations discussed above and below yield well-defined problems, it is not evident that the solution of such problems in the limit  $\lambda \rightarrow 0$  would automatically approach the correct shape. However, in cases where the boundary of the object is an occluding boundary one of  $p$  and  $q$  will become infinite and cannot therefore be used directly as boundary information. Previously to the effort of [11], Ikeuchi & Horn [13] presented a scheme where surface orientation is parameterized using stereographic co-ordinates,  $(f, g)$ . Such co-ordinates remain finite on occluding boundaries so that the values of  $f$  and  $g$  on the object boundary may be used as Dirichlet conditions for the problem. Unfortunately, there is a drawback in that the integrability condition cannot easily be expressed in stereographic co-ordinates. In order to obtain a unique solution, Ikeuchi & Horn considered the addition of a smoothing term and hence set out to minimize the functional

$$\iint \{\lambda(f_x^2 + f_y^2 + g_x^2 + g_y^2) + (E - R(f, g))^2\} d\Omega \quad (9)$$

Again, these equations were solved using a simple Jacobi iteration. Having obtained  $f$  and  $g$  these were then converted to  $(p, q)$  co-ordinates and  $z$  was computed as per (6). It should be noted that minimizing both (6) and (9) lead to nicely elliptic problems. A successful

implementation of multigrid methods applied to this scheme has been reported by Terzopoulos [17]. However, again it must be stressed that this scheme is essentially solving a different problem, since integrability is not imposed.

A number of schemes have been proposed in the form of a two-stage iteration, where in the first stage an approximate solution for  $p$  and  $q$  is obtained somehow and in the second stage this solution is projected onto one satisfying the integrability constraint. Most notable among these is the scheme of [7] which uses trigonometric polynomial expansions. Of course, some of the schemes described here earlier, e.g. [13], followed by a solution of (6), can also be viewed as one such iteration. Convergence proofs for these iterations are generally unavailable, though.

Finally, in [9] Horn presents a scheme which couples together the processes of determining an orientation map and of determining the depth map which had hitherto been dealt with sequentially. Thus one seeks functions  $z$ ,  $p$  and  $q$  which minimize the functional

$$\int \int_{\Omega} \{ \lambda (p_x^2 + p_y^2 + q_x^2 + q_y^2) + \mu [(z_x - p)^2 + (z_y - q)^2] + (E - R(p, q))^2 \} d\Omega \quad (10)$$

The first of these terms represents a departure from smoothness penalty term. In cases where there is little or no noise in the image it is expected that  $\lambda$  may be taken small or even reduced to zero. The second term is the integrability penalty term. The corresponding Euler equations are

$$\left. \begin{aligned} \lambda \nabla^2 p + \mu (z_x - p) + (E - R) R_p &= 0 \\ \lambda \nabla^2 q + \mu (z_y - q) + (E - R) R_q &= 0 \\ \nabla^2 z &= p_x + q_y \end{aligned} \right\} \quad (11)$$

Note that the non-elliptic integrability penalty term is now of lower order than the elliptic smoothness penalty term, in contrast to the earlier scheme consisting of minimizing the functional (8) plus (7).

Horn discretizes these equations on staggered grids – the grid for  $z$  being offset from the one for  $p$  and  $q$  by a 1/2 cell.

## 4 A multigrid algorithm

Because of the advantages of the regularization (10) for the application of a fast-but-fussy method like multigrid, we have chosen to concentrate on it. For the discretization, however, we adopt an alternative approach to [9] and discretize the integral (10) directly. Thus, we divide (an approximation of) the domain  $\Omega$  into a set of square cells. Let  $\Omega_{ij}$  be a square whose vertices are at points given by the cross products of  $x_{i-1}$ ,  $x_i = x_{i-1} + h$  and  $y_{j-1}$ ,  $y_j = y_{j-1} + h$ , with solution unknowns  $z_{ij} \approx z(x_i, y_j)$  etc. as usual. We approximate

$$\int \int_{\Omega_{ij}} \{ \lambda (p_x^2 + p_y^2 + q_x^2 + q_y^2) + \mu [(z_x - p)^2 + (z_y - q)^2] + (E - R(p, q))^2 \} dx dy$$

by

$$\frac{\lambda}{2h^2} [(p_{i,j-1} - p_{i-1,j-1})^2 + (p_{i,j} - p_{i-1,j})^2 + (p_{i-1,j} - p_{i-1,j-1})^2 + (p_{i,j} - p_{i,j-1})^2]$$

$$\begin{aligned}
& + (q_{i,j-1} - q_{i-1,j-1})^2 + (q_{i,j} - q_{i-1,j})^2 + (q_{i-1,j} - q_{i-1,j-1})^2 + (q_{i,j} - q_{i,j-1})^2 \\
& + \frac{\mu}{2} [(h^{-1}(z_{i,j-1} - z_{i-1,j-1}) - (p_{i,j-1} + p_{i-1,j-1})/2)^2 + (h^{-1}(z_{i,j} - z_{i-1,j}) \\
& - (p_{i,j} + p_{i-1,j})/2)^2 + (h^{-1}(z_{i-1,j} - z_{i-1,j-1}) - (q_{i-1,j} + q_{i-1,j-1})/2)^2 \\
& + (h^{-1}(z_{i,j} - z_{i,j-1}) - (q_{i,j} + q_{i,j-1})/2)^2] \\
& + \frac{1}{4} [(E_{i-1,j-1} - R(p_{i-1,j-1}, q_{i-1,j-1}))^2 + (E_{i,j-1} - R(p_{i,j-1}, q_{i,j-1}))^2 \\
& + (E_{i-1,j} - R(p_{i-1,j}, q_{i-1,j}))^2 + (E_{i,j} - R(p_{i,j}, q_{i,j}))^2] =: F_{ij}
\end{aligned} \tag{12}$$

Then, consider the minimization of

$$F := \sum_{i,j} F_{ij} \tag{13}$$

and equate the derivative of  $F$  with respect to each unknown to zero, as a necessary condition for a minimum. (The obtained averages for  $p$  and  $q$  may be lumped in an obvious way.)

This naturally leads to a 2nd order discretization of (11) on non-staggered grids. It can be shown that the resulting discrete system has a good  $h$ -ellipticity measure (see Brandt & Dinar [3]) when  $\lambda = 0$ , whereas the staggered grid scheme does not. Dirichlet boundary conditions are handled by fixing the corresponding grid unknowns. Neumann boundary conditions, when there are any, are handled naturally, as part of the above process. This does not slow down the multigrid iteration, as compared to the case with Dirichlet conditions.

Furthermore, we employ an FMG continuation algorithm in  $\lambda$  as demonstrated in Figure 1. On the coarsest level we start with a value of  $\lambda$  which is large enough to ensure a good smoothing rate. A hierarchy of embedded grids with square cells is used with the usual coarse/fine width ratio of 2. When proceeding to a new finest grid the value of  $\lambda$  is reduced by a factor of 4, so that  $\bar{\lambda} := \lambda/h_f^2$  remains constant, where  $h_f$  is the currently finest grid width. For each finest grid in turn we apply one nonlinear (FAS [2])  $W(2,2)$  cycle, using a collective Gauss-Seidel (CGS) relaxation with one Gauss-Newton iteration for the nonlinear term  $(E - R(p, q))^2$  (treated pointwise) and the usual bilinear interpolation and its adjoint full-weighting restriction. An initial guess at the solution on a new finest level is obtained using bi-cubic interpolation. Having reached the finest level, 4  $W(2,2)$  cycles are performed in order to finish the method's application.

Note that we do not change the value of  $\lambda$  within a cycle. Thus, at least for  $\lambda \sim 1$  the usual multigrid theory and experience imply that a fast solver is obtained. In this case we have at the given stage of the continuation process a standard (FAS) nonlinear multigrid method applied to the diagonally dominant elliptic system (11). Rapid convergence in this case has been confirmed in our experiments. However, to avoid extra smoothing of the solution features one has to consider small values of  $\lambda$  when  $h_f$  is small. The FMG- $\lambda$  continuation process turns out then to be essential for obtaining good approximate solutions for (12)-(13) with so few relaxations on the finest grid for a very small  $\lambda$ , as reported in the next section.

The idea behind refining  $\lambda$  such that  $\bar{\lambda}$  remains constant corresponds to the usual procedure when approximating noisy data. Thus, in the first two equations in (11) the sizes of the smoothing terms retain a fixed ratio to the sizes of the data fit residuals.

With the CGS Gauss-Newton relaxation the choice of  $\mu$  for a given small  $\lambda$  must be neither



with  $L = 1, 2$  or  $3$ . The same discretization and the same multigrid algorithm as described earlier are employed.

More images add information, of course, so we expect better shape recovery. If at each point of the domain there are at least two images with nonzero brightness, and if there is no noise, then the minimum of (15) with  $\lambda = 0$  is 0 and the gradient  $(p, q)$  can be found pointwise. (In case of 3 images we can even write an explicit expression for the Lambertian-model gradient.) However, we do not use such specific information here, since we are really interested in the more general case and consider such specialized situations as synthesized noise free multiple images merely in order to sort out the various possible difficulties which may arise.

## 5 Selected test results

The algorithm described in Section 4 has been tested on a synthetically generated image of a Lambertian spherical cap merging smoothly into a constant background, as well as on a synthetic vase and on "real" images of pottery vases [19], one of which is presented here. For the "real" images it has been assumed that the object has reflectance properties that are closely modelled by a Lambertian surface. This allows for the use of the analytic, nonlinear form (3) for  $R$ . Hence, for these images we have potential not only for noise in the image itself (i.e. in  $E(x, y)$ ) but also for errors in modelling the reflectance map  $R(p, q)$ . Incorporating the background presents an additional difficulty, because that material may well have a different reflectance map.

Below we report the results of applying the multigrid algorithm just described, using 7 or 8 grids in all cases, with the finest grid having  $128 \times 128$  or  $256 \times 256$  cells, respectively. In all cases we have chosen  $\lambda$  on the coarsest grid so that the  $\lambda$ -term is at least the order of the  $\mu$ -term in (11) and ended up with  $\lambda \ll \mu$  on the finest grid. Our choices for  $\mu$  in (10) varied in the range 0.01-0.5. The values of  $\bar{\lambda} = \lambda/h_j^2$  and  $\mu$  used in each case are given in the figure captions.

### 5.1 One synthetic image, rectangular image boundary

Our first set of experiments is performed on a smooth, synthetic image. The data is generated as follows: For  $-0.5 \leq x, y \leq 0.5$  we use

$$z(x, y) = z(r \cos \phi, r \sin \phi) = f(r) \quad 0 \leq \phi \leq 2\pi$$

where  $f(r)$  describes a circular arc "taped" to the  $r$ -axis by a quadratic, forming a  $C^1$  function. Depending on three parameters  $0 < \beta < \alpha \leq 1$  and  $\rho \leq 0.5$ ,  $f$  is given by

$$f(r) = \begin{cases} \sqrt{\rho^2 - r^2} - \rho\sqrt{1 - \alpha^2} & r < \beta\rho \\ ar^2/(\beta\rho) - br + \rho c & \beta\rho \leq r < \gamma\rho \\ 0 & r \geq \gamma\rho \end{cases}$$

$$a = \frac{\beta^3}{4(1 - \beta^2)(\sqrt{1 - \beta^2} - \sqrt{1 - \alpha^2})}, \quad b = 2a + \frac{\beta}{\sqrt{1 - \beta^2}}$$

$$c = \frac{\beta b^2}{4a}, \quad \gamma = \beta + \frac{\beta^2}{2a\sqrt{1-\beta^2}}$$

Figure 2 shows the surface  $z$  as well as the synthetic image constructed by

$$E(x, y) := R(z_x, z_y)(x, y)$$

for the parameter values  $\alpha = 0.85, \beta = 0.7, \rho = 0.33$  using a Lambertian model (3). These yield a maximum value  $z(0, 0) = 0.156$ .

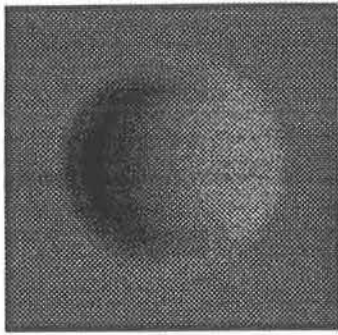
In Table 1 we display results of several runs using 7 grids as described above for various parameter values of  $\bar{\lambda}$  and choices of Dirichlet or natural boundary conditions for  $z$  and its gradient. The starting guess on the coarse grid is  $p = q = z = 0$ . The final average residual observed after 4 cycles for the finest grid is recorded under 'residual', and the average error in the obtained surface is recorded under 'error'.

$\lambda$	$\mu$	BC- $z$	BC- $(p, q)$	residual	error
4.0	0.5	Dirichlet	Dirichlet	$2.0 \times 10^{-6}$	$7.5 \times 10^{-3}$
4.0	0.5	Dirichlet	Natural	$2.0 \times 10^{-6}$	$8.1 \times 10^{-3}$
4.0	0.5	Natural	Dirichlet	$3.0 \times 10^{-6}$	$3.9 \times 10^{-2}$
4.0	0.5	Natural	Natural	$2.0 \times 10^{-6}$	$2.9 \times 10^{-2}$
0.4	0.5	Dirichlet	Dirichlet	$3.2 \times 10^{-4}$	$2.3 \times 10^{-3}$
0.4	0.5	Dirichlet	Natural	$2.2 \times 10^{-4}$	$2.4 \times 10^{-3}$
0.4	0.5	Natural	Dirichlet	$5.6 \times 10^{-4}$	$1.2 \times 10^{-2}$
0.4	0.5	Natural	Natural	$3.4 \times 10^{-4}$	$1.9 \times 10^{-2}$
0.04	0.5	Dirichlet	Dirichlet	$2.4 \times 10^{-3}$	$1.7 \times 10^{-3}$
0.04	0.5	Dirichlet	Natural	$1.3 \times 10^{-3}$	$1.6 \times 10^{-3}$
0.04	0.5	Natural	Dirichlet	$4.0 \times 10^{-3}$	$4.8 \times 10^{-3}$
0.04	0.5	Natural	Natural	$3.5 \times 10^{-2}$	$6.1 \times 10^{-2}$

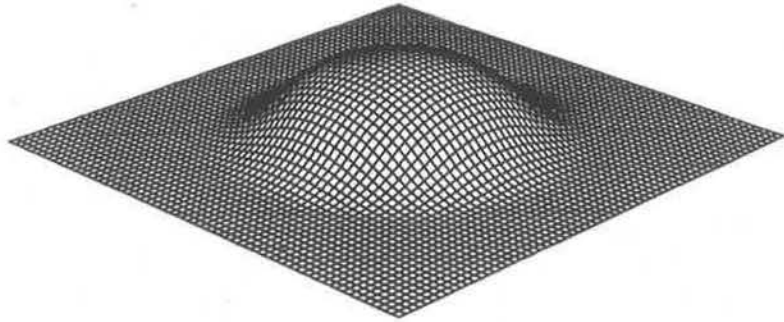
Table 1: Parameters and errors for the smoothed cap

From these results it is evident that the efficiency of the proposed algorithm is satisfactorily high so long as  $\bar{\lambda}$  does not become too small. The obtained accuracy in  $z$  improves, however, as  $\bar{\lambda}$  is decreased. This is hardly surprising, since the image under consideration is smooth with no noise present. The obtained results for the case  $\bar{\lambda} = 0.04$  are shown in Figure 3: In (i) the computed  $p$  and  $q$  are inserted into the reflectance map, and the result plotted, using the same light source direction as the input; in (ii) the reflectance map into which the computed  $p$  and  $q$  are inserted is for a different light source direction; and in (iii) a plot of the reconstructed surface  $z$  is displayed. In these runs Dirichlet boundary conditions ( $z = p = q = 0$ ) were employed on the square boundary of the image.

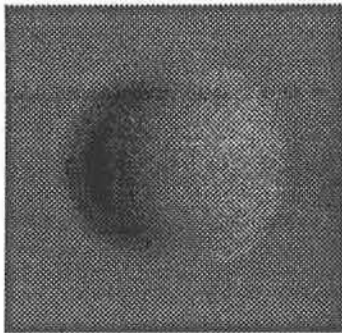
We also observe that the results for the case where natural boundary conditions are imposed on all solution components are worse than in other cases (even though the multigrid performance is not seriously affected). The effect is disastrous in the obtained  $z$ -surface for  $\bar{\lambda} = 0.04$  (i.e. the surface is rather distorted).



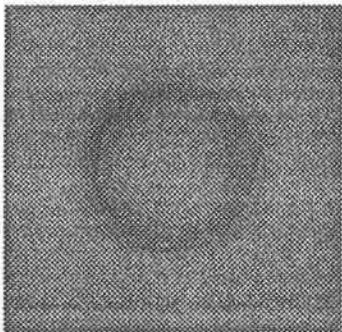
(i)



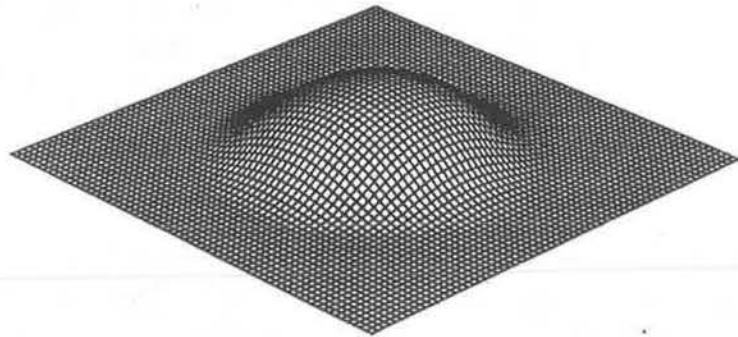
(ii)

Figure 2: Synthetic Image  $128 \times 128$  : (i) Input image (ii) Exact surface

(i)



(ii)



(iii)

Figure 3: Synthetic Image  $128 \times 128$ ,  $\bar{\lambda} = 0.04$ ,  $\mu = 0.5$ : (i) Reconstructed brightness (same light source as input) (ii) Reconstructed brightness (overhead illumination) (iii) Computed surface

In Figures 2 and 3 of [1] we show results of our algorithm applied to images of a synthetic hemisphere and to a “real” vase. Unlike the object of Figures 2 and 3 of the present paper, those images contain edges along which the surface may be discontinuous. It was observed that although the algorithm does a reasonably good job of solving the image irradiance equation, the boundary of the object was seriously smoothed away and the reconstructed object was severely flattened. The smoothing of the object’s boundary is expected, since the approximate solutions for  $z$ ,  $p$  and  $q$  are sought in  $H^2(\Omega)$ , whereas the exact  $z$  is discontinuous across an occluding boundary and at least one of  $p$  and  $q$  is infinite there. Moreover, the reflectance map  $R$  is not always sensitive to large changes in the gradient (in the absolute sense) to which the recovered surface  $z$  is more sensitive. (This may give an intuitive feeling for the many efforts [10] which proceed at first to find the orientation and only then to find the surface itself.)

In the next subsection we therefore introduce discontinuities into the model as described earlier. The locations of these discontinuities are assumed to be part of the given data (they are formed by an edge detector applied to the brightness data). This implies that we now must consider objects with natural boundary conditions for which, Table 1 suggests, difficulties may arise. We therefore seek to improve the quality of the recovered surface by using two or three images instead of one, which allow a much better recovery of accurate orientation.

## 5.2 Allowing discontinuities

In Figure 4 we show 3 input brightness maps which correspond to one synthetic object, lit from different light source directions. The “synthetic vase” object (Figure 4 (iv)) was obtained as a surface of revolution based on a silhouette curve which is a polynomial of degree 6 with maximum  $z = 0.27$ . We apply the algorithm described in Section 4 to the discretization of (15) with  $L = 2$  (using images (i) and (ii) of Figure 4) and  $L = 3$  (using image (iii) also).

While the results are better than can be expected with one image, we note that convergence problems in the limit  $\lambda \rightarrow 0$  do not completely disappear: as observed before, convergence of the relaxation becomes a serious issue. Also, in regions where one of the images is dark (e.g. the right side of the vase in Figure 4 (i) - the brightness there is  $E_1 = 0$ ) information is only available from the other image(s). It is important to refrain from applying “stabilizing” mechanisms which may yield rapid convergence but at the same time produce a distorted surface. One example of such a poor stabilization is adding a term  $\nu(p^2 + q^2)$ ,  $\nu$  a nonnegative parameter, to the functional (15). Also, the Lambertian reflectance map may become negative while the brightness is nonnegative. Allowing this improves convergence for the case with 3 input images, but again causes distortion where one of the images is dark. We therefore set

$$R(p, q) \leftarrow \max(R(p, q), 0)$$

(and  $\nu = 0$ ) which yields the slower convergence but better results of Figure 6 below.

Results for  $\bar{\lambda} = 0.4, \mu = 0.01$  using two images are displayed in Figure 5. As usual, distortions show up more clearly in the reconstructed surface than in the reconstructed brightness maps. The “neck” of the vase is largely smoothed away. In contrast, the residual for  $\bar{\lambda} = 0.4, \mu = 0.01$  with 3 images is larger, residual = 0.206, but error = 0.01. The recon-

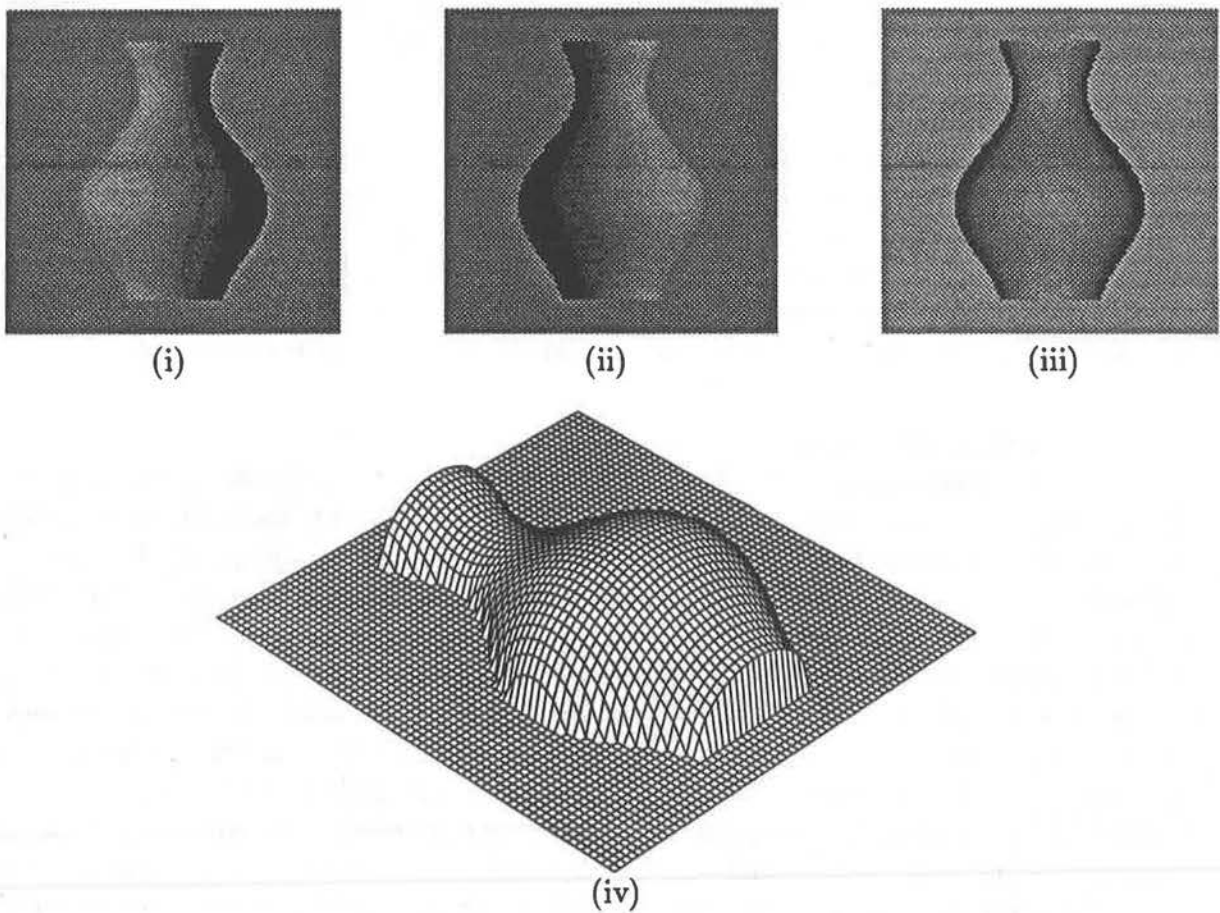


Figure 4: Synthetic Vase  $128 \times 128$  : (i), (ii) & (iii) Input images (iv) Exact surface

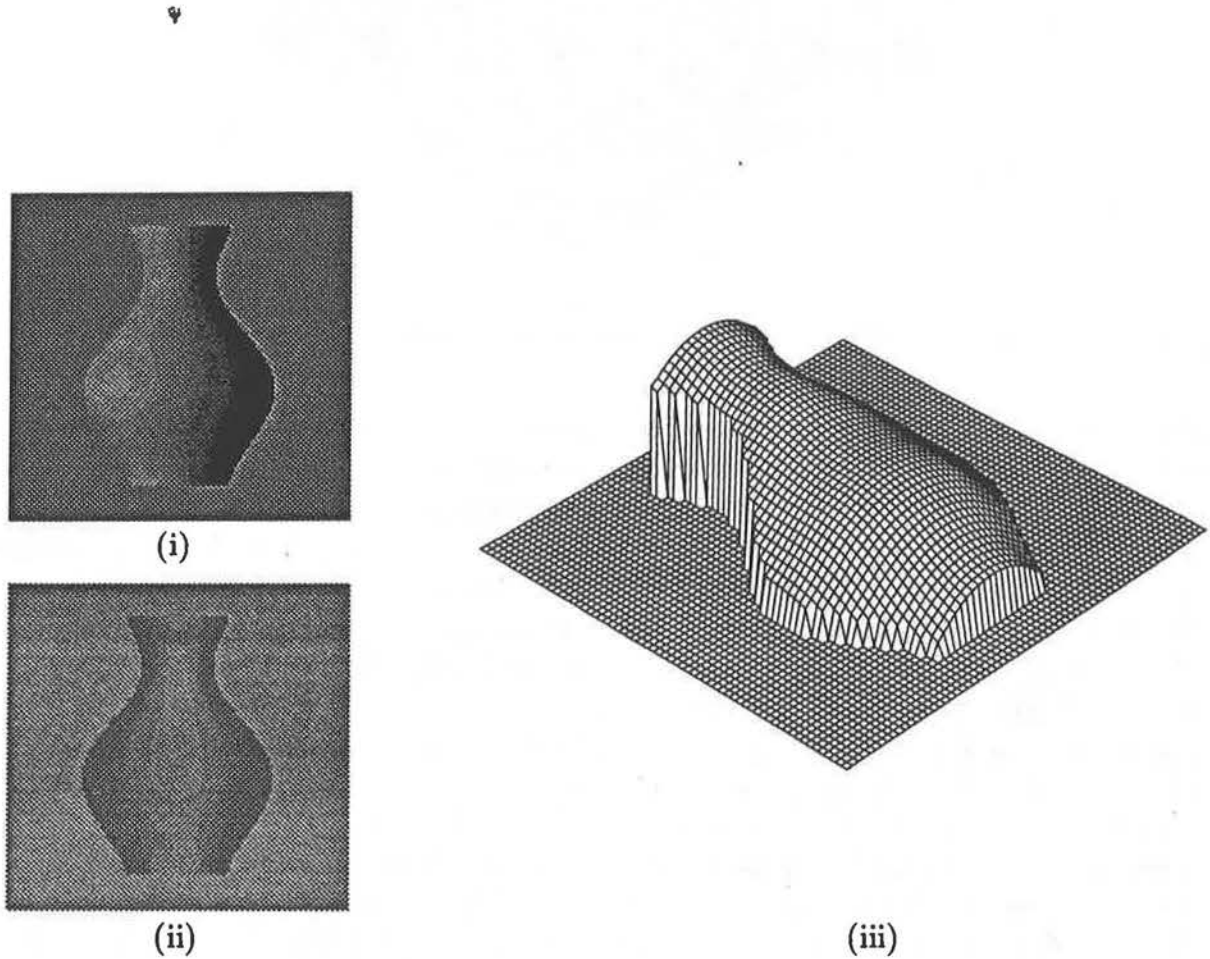


Figure 5: Synthetic Vase  $128 \times 128$ , two input images,  $\bar{\lambda} = 0.4$ ,  $\mu = 0.01$ : (i) Reconstructed brightness (same light source as input) (ii) Reconstructed brightness (overhead illumination) (iii) Computed surface

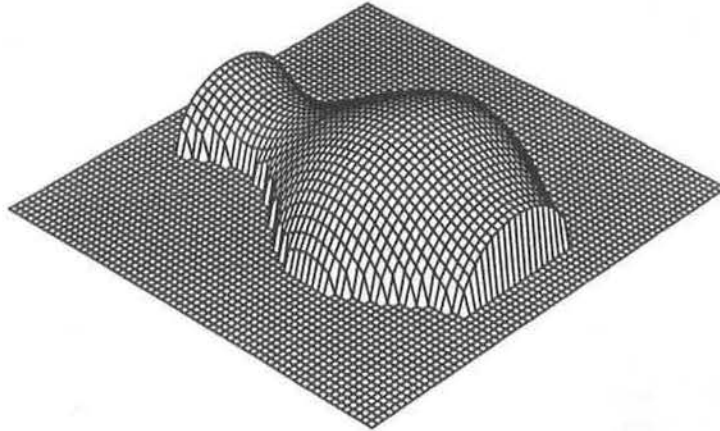


Figure 6: Synthetic Vase  $128 \times 128$ , three input images,  $\bar{\lambda} = 0.4$ ,  $\mu = 0.01$ : Computed Surface

structured surface is displayed in Figure 6. It is in excellent agreement with the original. We emphasize again, though, that this is a synthetic image with no noise.

Finally, in Figure 7, we display results of our algorithm applied to real data, as described at the beginning of this section. The two input images are not very different from the displayed output but the computed surface is flattened much like the synthetic image in Figure 5.

Unlike previous calculations reported here, the integration for Figure 7 is done only on the object area, with the background held fixed (and the object fixed at one point at an appropriate height above the background).

The reasons for the errors in the solution of Figure 7 are likely due to the following: (i) Errors in modelling the reflectance map – it is unlikely that for the real images, the surface of the pottery vases is exactly modelled by an ideal Lambertian surface; (ii) Errors in the image data, which are not precisely compensated for by any choice of  $\lambda$  (i.e., the mathematical problem does not exactly correspond to the underlying physical problem); (iii) The exact solution we are trying to compute becomes infinite at the boundary of the object – that is surface slopes become infinite at an occluding boundary. Work is currently under way to address these issues, as well as attempting to obtain a more robust method if data is given for only one image.

**Acknowledgement:** The data for the “real” vase images which we have used was kindly provided to us by Professor Bob Woodham. We are also indebted to him for many fruitful discussions.

## References

- [1] Ascher U. & Carter P., “Multigrid Solution for Shape from Shading”, in Proceedings Third European Conference on Multigrid Methods, Bonn, 1990.

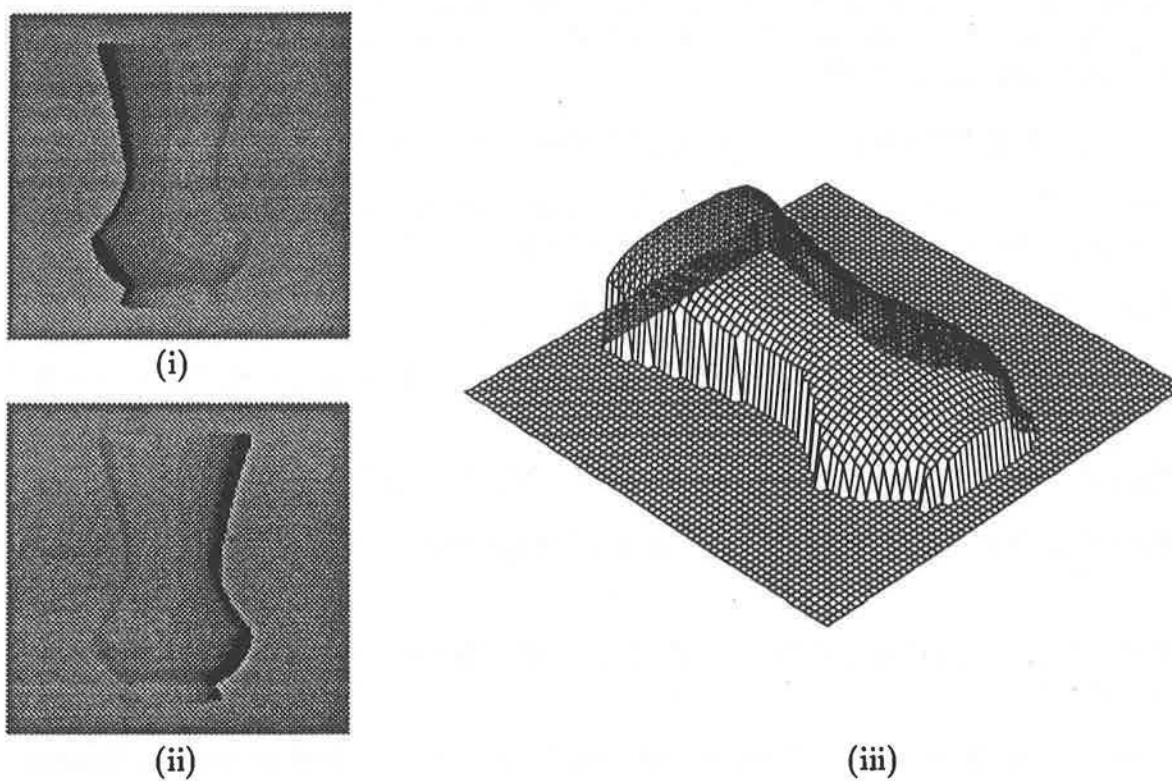


Figure 7: "Real" Image  $128 \times 128$ ,  $\bar{\lambda} = 0.4$ ,  $\mu = 0.01$ : (i) & (ii) Reconstructed brightness (same light source as input) (iii) Computed surface

- [2] Brandt A., "Guide to Multigrid Development", in *Multigrid Methods* eds. W. Hackbusch and U. Trottenberg, Proceedings of Conference on Multigrid Methods, Koln-Porz, 1981.
- [3] Brandt A. & Dinar N., "Multigrid Solutions to Elliptic Flow Problems", in *Numerical Methods for Partial Differential Equations*, ed. S. Parter, Proceedings, Oct 1978. Academic Press 1979.
- [4] Brooks M.J., Chojnacki W. & Kozera R., "Shading Without Shape", TR 90-10, Computer Science, Flinders University, Adelaide, Australia, 1990.
- [5] Brooks M.J., Chojnacki W. & Kozera R., "Spherically Symmetric Eikonal Equations and Nonuniqueness in Computer Vision", TR 90-11, Computer Science, Flinders University, Adelaide, Australia, 1990.
- [6] Courant R. & Hilbert D. *Methods of Mathematical Physics*, Interscience, 1953.
- [7] Frankot R.T. & Chellappa R., "A Method for Enforcing Integrability in Shape From Shading Algorithms", IEEE Trans. PAMI 10 1988, 439-451.
- [8] Horn B.K.P., *Robot Vision*, MIT Press 1986.
- [9] Horn B.K.P., "Height and Gradient from Shading", Int. J. of Computer Vision 5 1990, 37-75.
- [10] Horn B.K.P. & Brooks M. (eds.), *Shape from Shading*, MIT Press 1989.
- [11] Horn B.K.P. & Brooks M., "The Variational Approach to Shape from Shading", CVGIP 33 1986.
- [12] Horn B.K.P. & Sjoberg R.W., "Calculating the Reflectance Map", Applied Optics 18 (11) 1979.
- [13] Ikeuchi K. & Horn B.K.P., "Numerical Shape from Shading and Occluding Boundaries", Artificial Intelligence 17 1981.
- [14] Marr D., *Vision*, Freeman & Co. 1982.
- [15] Ramachandran V.S., "Perceiving Shape from Shading", Scientific American, August 1988.
- [16] Sweldens & Roose, in Proceedings Third European Conference on Multigrid Methods, Bonn, 1990.
- [17] Terzopoulos D., "Image Analysis using Multigrid Relaxation Methods", IEEE PAMI 8 (2) 1986.
- [18] Woodham R.J., "Photometric Method for Determining Surface Orientation from Multiple Images", Optical Engineering 19 (1) 1980.

- [19] Woodham R.J., "Determining Surface Curvature with Photometric Stereo", Proceedings of 1989 IEEE Conference on Robotics and Automation, Scottsdale, Arizona.

Uri M. Ascher  
Dept. of Computer Science,  
University of British Columbia,  
Vancouver, B.C., V6T 1W5,  
CANADA.

Paul M. Carter  
Dept. of Mathematics,  
University of British Columbia,  
Vancouver, B.C., V6T 1Y4,  
CANADA.